Int. J. Heat Mass Transfer. Vol. 34, No. 7, pp. 1679–1693, 1991
Printed in Great Britain

0017-9310/91 $3.00+0.00

Natural convection from two-dimensional discrete heat sources in a rectangular enclosure

M. L. CHADWICK, B. W. WEBB and H. S. HEATON
Mechanical Engineering Department, Brigham Young University, Provo, UT 84602, U.S.A.

(*Received* 29 *January* 1990 *and in final form* 9 *August* 1990)

Abstract—Natural convection in a discretely heated enclosure is investigated experimentally and theoretically for single and multiple heater configurations. Mach–Zehnder interferometry is used to visualize the temperature field within the enclosure and to determine the local and average heat transfer characteristics of the discrete heat sources. The partial differential equations governing the conservation of mass, momentum and energy for the problem are solved numerically. The results show that for the single heat source configuration heater locations closer to the bottom of the enclosure yield the highest heat transfer in the high Grashof number range. However, the observation of previous work that the heat source location corresponding to maximum heat transfer is a function of Grashof number is confirmed. Discrete heat sources located near the enclosure bottom are also found to yield the highest heat transfer in the dual heater configuration. The heater placement for maximum heat transfer in both single and dual heater systems is explained in terms of the intensity of the buoyancy-driven flow in the enclosure. The thermal wake of the bottom heat source is seen to significantly affect the transport from heat sources above in the multiple heat source configurations. The lowest heat source, however, is influenced only marginally by the presence of a heater above.

INTRODUCTION

THE INCREASING miniaturization of electronic components and the resultant rise in heat flux density has spawned the need for better understanding of the fundamentals of heat transfer in discrete heating situations. Passive (natural convective) cooling of electronic equipment continues to play a prominent role in the thermal management and control of such systems. Natural convection cooling techniques have distinct advantages because of their low cost, ease of maintenance and absence of electromagnetic interference and operating noise [1, 2]. In some situations the heat sources must be isolated from the exterior environment. The configuration is then described by natural convection in an enclosure with discrete heat sources.

Chu *et al.* [3] appear to be the first to have studied natural convection heat transfer from a discrete heat source in a two-dimensional enclosure. The numerical study investigated the effect of size and location of a single heater for a range of Grashof numbers. The local and average heat transfer were found to be strongly dependent on heater location. A maximum in average Nusselt number as a function of heater distance from the top of the cavity was observed, and the location corresponding to maximum heat transfer was found to be a function of Grashof number. The numerical predictions of Chu *et al.* were later corroborated experimentally by Turner and Flack [4], who later correlated the heat transfer data as well [5].

More recently, Keyhani *et al.* [6, 7] investigated experimentally the buoyancy-driven flow and heat transfer characteristics of an array of discrete heat sources in enclosures of aspect ratios 4.5 and 16.5. They found that a discretely heated vertical cavity yielded significantly enhanced heat transfer over a fully heated vertical wall. The experiments revealed strong secondary and tertiary flows which resulted in higher heat transfer. A subsequent numerical study [8] revealed the influence of aspect ratio and size of heat source on the natural convection in a discretely heated cavity.

A number of investigations have treated the effects of protrusion of the discrete heat sources during natural convection cooling in enclosures. The studies have approached the problem from both experimental [9–11] and analytical [12] perspectives. In general, these studies illustrate the penetration of the flow into the gaps separating the protruding heat sources.

This paper presents results of an experimental and analytical study of natural convection in a vertical cavity with single and multiple flush-mounted, two-dimensional discrete heat sources. This study supplements the results of earlier work in that the local and average heat transfer characteristics of single and multiple discrete heater configurations are quantified and correlated, and the influence of the thermal wake in multiple discrete heater systems is illustrated. The problem parameters investigated in the study include Grashof number, heat source location(s), and cavity aspect ratio for single and multiple heater enclosures. The Grashof number range is extended beyond that studied previously. Mach–Zehnder interferometry was used to determine the local heat transfer in the experiments.

APPARATUS

The enclosure used in the experimental study is shown schematically in Fig. 1. The two-dimensional

NOMENCLATURE

g	gravitational acceleration
Gr	modified Grashof number based on heater height, $g\beta qL^4/kv^2$
$Gr_{y'}$	local modified Grashof number based on distance from leading edge of heater, $g\beta q(y')^4/kv^2$
h	local heat transfer coefficient, $q/(T-T_w)$
H	height of enclosure
k	thermal conductivity
L	length of heater
L_{uh}	length of unheated section between multiple discrete heat sources
Nu	local Nusselt number, hL/k
$Nu_{y'}$	local Nusselt number based on distance from leading edge of heater, hy'/k
$\overline{Nu}$	average Nusselt number, equation (6)
Pr	Prandtl number, v/α
q	convective heat flux at heater surface
Ra	modified Rayleigh number, $Gr\,Pr$
s	distance from the top of the enclosure to the midpoint of the heater
T_w	temperature of isothermal wall
U	dimensionless velocity in the x-direction, uL/v
V	dimensionless velocity in the y-direction, vL/v
X	dimensionless distance in the x-direction, x/L
Y	dimensionless distance in the y-direction, y/L
W	width of enclosure.

Greek symbols

β	volumetric coefficient of thermal expansion
θ	dimensionless temperature, $(T-T_w)/(qL/k)$
v	kinematic viscosity
Ψ	dimensionless stream function, ψ/v.

Subscripts

H	based on enclosure height
W	based on enclosure width.

enclosure used in the experimental studies was 19.05 cm tall with variable widths of 3.18, 3.81, and 4.76 cm. The cavity was 30.48 cm in the spanwise direction, ensuring near two-dimensionality of the flow and heat transfer. The horizontal surfaces were maintained nearly adiabatic by constructing them of closed-pore, extruded polystyrene insulation. A constant temperature boundary was imposed at the other vertical surface; pure copper was used for the constant temperature (isothermal) wall. Channels were milled in the copper slab in a counterflow arrangement. Coolant was pumped through the channels and the temperature of the coolant was controlled by a constant temperature bath. Thermocouples were embedded in the copper wall and monitored to ensure a uniform temperature distribution. The maximum temperature variation was found to be 0.1°C across the copper wall. Optical quality glass was used for the spanwise vertical walls of the cavity to allow interferometric access to the interior of the enclosure.

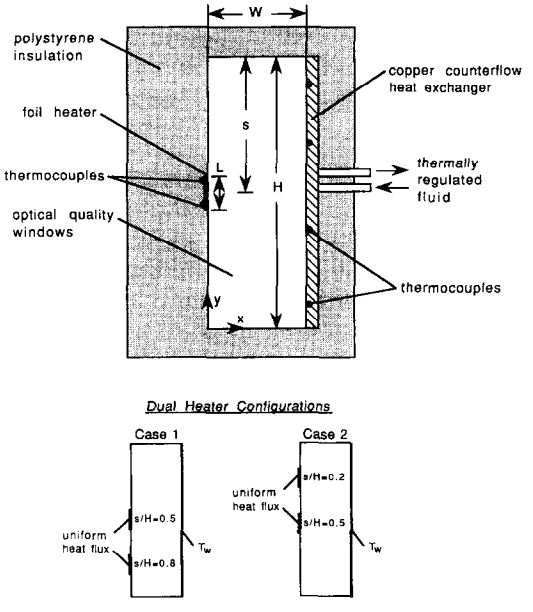

FIG. 1. Schematic of experimental apparatus and definition of geometric parameters.

The aspect ratio of the cavity, H/W, was varied by sliding the discretely heated wall horizontally relative to the isothermal wall, thus varying the width of the enclosure (W). For the single heater, a single aspect ratio of $H/W = 5$ was studied. Aspect ratios of $H/W = 4$, 5, and 6 were investigated in the dual heater configuration.

Strips of 0.0025 cm thick stainless steel shim stock were used as resistive heater elements. The heater length for all cases was $L = 2.54$ cm. The Grashof number was varied by changing the heat flux imposed at the heat source. Aluminum busbars were used to transmit power from a d.c. power supply to the heater strips. The stainless steel shim stock heater material was sandwiched between a single, heavy aluminum busbar and a mating slab of non-conductive material. An electrically conducting paint with dissolved nickel shavings was applied between the busbar and the shim stock to reduce the electrical contact resistance. The busbar system extended the entire height of the cavity

at both spanwise extremities, permitting the heat source(s) to be placed at any vertical location. Felt was glued to the busbar assembly surface exposed to the optical glass at both ends of the cavity to reduce heat losses. Dimensionless heater locations of $s/H = 0.2$, 0.5, and 0.8 were studied for the single heater configuration, while heater locations of $s/H = 0.2$ and 0.5, and 0.5 and 0.8 were investigated in the dual heater system.

Ohmic heating in the heater strips was achieved by passage of an electrical current through the stainless steel shim stock from a 20 V, 120 A d.c. power supply stable to 0.1%. The electrical power dissipated in each heater strip was calculated by the product of the voltage (measured directly to within 0.01 V on the heater foil with voltage taps) and the current read from the power supply to within 0.1 A. Identical electrical power was delivered to the two heater strips in the dual heater configuration. After power was applied to the heater strip(s), thermocouples mounted at various positions under the heat source(s) were monitored to determine when the system had reached steady state. Typically, 20 h were required to reach steady state when starting from a cold enclosure assembly.

A Mach–Zehnder interferometer with 30.5 cm optics was used to visualize the temperature field and to quantify the local heat transfer along each heat source. The interferometer is of parallelogram design in a 60° configuration. The interferometer was set initially to an infinite fringe mode and changes in the index of refraction of the air, within the enclosure, were seen as interference fringes. The fringe pattern was recorded photographically using a 10.2 cm × 12.7 cm format camera and exposing the image directly on to the negative at a shutter speed of 1/60 s. The photographically recorded interferograms were interpreted using established optical techniques [13]. For the interferograms presented hereafter the temperature difference corresponding to each fringe shift was approximately 2.9°C.

A measuring microscope, with a spatial resolution of 2.5 μm, was used to measure the distance between fringes near the heater. The variation in fluid temperature with distance from the heat source was represented by a curve-fit of the interference fringe data using a second-order polynomial. In general, four to six fringes were used in the regression depending on fringe density in the Mach–Zehnder interferograms. The local wall convective heat flux was calculated by evaluating the first derivative of the polynomial curve fit at the wall. The local heat source temperature was determined by evaluating the polynomial itself at the wall. This evaluation was performed at nine vertical locations along each heater strip to determine the variation of the local Nusselt number. Nusselt numbers determined in this way are based only on the convective heat flux, and did not include radiation, since the local convective heat transfer from the heat sources was determined directly from the measured temperature gradient in the fluid. Since radiation heat transfer constituted a fraction of the total heat transfer from the heater strip(s), the Grashof number characterizing each experimental condition was based on the average convective heat flux over each heat source.

An error analysis using the method of Kline and McClintock [14] was performed, from which it was found that the maximum uncertainties in the local Nusselt and Grashof numbers were, respectively, 7.8 and 8.7%.

ANALYSIS

Under the assumptions of steady, laminar, natural convection of a Newtonian fluid with changes in fluid density treated using the Boussinesq approximation, the dimensionless partial differential equations governing transport of mass, momentum, and energy in the discretely heated enclosure are, respectively:

continuity

$$\frac{\partial U}{\partial X} + \frac{\partial V}{\partial Y} = 0; \tag{1}$$

X-momentum

$$U\frac{\partial U}{\partial X} + V\frac{\partial U}{\partial Y} = \frac{\partial^2 U}{\partial X^2} + \frac{\partial^2 U}{\partial Y^2} - \frac{\partial P}{\partial X}; \tag{2}$$

Y-momentum

$$U\frac{\partial V}{\partial X} + V\frac{\partial V}{\partial Y} = \frac{\partial^2 V}{\partial X^2} + \frac{\partial^2 V}{\partial Y^2} - \frac{\partial P}{\partial Y} + Gr\,\theta; \tag{3}$$

energy

$$U\frac{\partial \theta}{\partial X} + V\frac{\partial \theta}{\partial Y} = \frac{1}{Pr}\left(\frac{\partial^2 \theta}{\partial X^2} + \frac{\partial^2 \theta}{\partial Y^2}\right). \tag{4}$$

The boundary conditions may be stated as follows:

$$Y = 0: \quad U = V = \frac{\partial \theta}{\partial Y} = 0 \tag{5a}$$

$$Y = H/L: \quad U = V = \frac{\partial \theta}{\partial Y} = 0 \tag{5b}$$

$$X = 0: \quad U = V = 0 \tag{5c}$$

$$\frac{\partial \theta}{\partial X} = -1 \text{ at heat source}$$

$$\frac{\partial \theta}{\partial X} = 0 \quad \text{elsewhere}$$

$$X = W/L: \quad U = V = \theta = 0. \tag{5d}$$

The coupled equations of mass, momentum, and energy, equations (1)–(4), were discretized and solved using a control volume based finite difference technique. The coupling between continuity and pressure was handled using the well-established SIMPLER algorithm [15]. The equations were solved on a 60 × 60 non-uniform grid with 20 control volumes on each heat source for the single and dual heat source systems. Nodes were clustered along the vertical walls

to better resolve the hydrodynamic and thermal boundary layers there. Refined grids of 80×80, 60×90, 60×112, and 60×158 nodes were used for the three, four, five, and continuous heat source simulations, respectively. These grid distributions were determined by successive refinements of an initial 20×20 grid until the average Nusselt number for each heater changed by less than 0.3%.

The average Nusselt number was calculated according to its definition for isoflux heating

$$Nu = \frac{qL}{k\overline{\Delta T}} \tag{6}$$

where the average wall temperature rise, $\overline{\Delta T}$, was determined by numerically integrating the local temperature data.

Note that previous investigators have based their Grashof number on the enclosure height, H. The Grashof number in this study was based on heat source height, L. This is significant because, as will be seen subsequently, the Grashof number range simulated in this study is several orders of magnitude higher than that examined in previous investigations [3, 4, 8]. The heat flux used in defining the Grashof number for the numerical simulation of the experiments was based on the average of the local convective heat transfer data over the length of the heater, determined from the Mach–Zehnder interferograms.

The dimensionless stream function was calculated from the velocity field according to their definitions

$$U = \frac{\partial \Psi}{\partial Y} \tag{7}$$

and

$$V = -\frac{\partial \Psi}{\partial X}. \tag{8}$$

RESULTS AND DISCUSSION

Results are categorized and presented as single heat source and dual heat source data. For the single heater configuration, one aspect ratio of $H/W = 5$ was studied analytically and experimentally with heater locations of $s/H = 0.2$, 0.5, and 0.8. Heater location and the characterization of its effect on the heat transfer was the objective of this portion of the work. For the dual heater system two cases were considered, including heater locations of $s/H = 0.5$ and 0.8 hereafter referred to as Case 1, and heater locations of $s/H = 0.2$ and 0.5, termed Case 2. With the dual heat source configuration, the effect of enclosure aspect ratio was studied analytically in the range $H/W = 2$–8 and experimentally for $H/W = 4$, 5, and 6. Once the analytical studies were compared to the experimental work and validated, multiple heat sources were studied theoretically for an aspect ratio of $H/W = 5$. Results are presented in terms of local and average Nusselt number distributions for both the experimental and theoretical work.

SINGLE HEAT SOURCE CONFIGURATION

Figure 2 shows a comparison between the experimental temperature field and theoretical predictions for temperature and flow field for an aspect ratio of $H/W = 5$ for the single heater location of $s/H = 0.8$. The predicted isotherms shown are uniformly incremented, although the dimensionless temperatures do not necessarily correspond to those in the Mach–Zehnder interferogram. The predicted isotherms are seen to be qualitatively similar to the experimental isotherms. The presence of a thermal boundary layer with isotherms clustered near the region of high heat transfer along the discrete heater is evident. The temperature of the heat source is seen to rise with increasing distance from its leading edge. This boundary layer developed for all the heater locations and Grashof numbers studied experimentally and analytically. The central region of the enclosure exhibits a thermally stable stratification, similar to the classical result for buoyancy-driven flow in an enclosure with differentially heated walls [16].

The predicted stream function was calculated for each numerical simulation to visualize the flow field within the enclosure. For the heat source location of $s/H = 0.8$, the fluid was heated at the discrete source, and rose due to buoyancy forces. The warmed fluid was then turned by the adiabatic ceiling of the enclosure and descended along the cooled wall, completing a recirculation flow pattern that occupied the entire enclosure. This recirculating flow pattern is clearly evident in Fig. 2, with the center of the primary eddy being at $y/H \approx 2/3$. A secondary recirculation zone was predicted in the upper left corner, indicative of separation of the flow originating from the heater and rising along the remainder of the adiabatic wall. The preferred flow structure seems to be this separation from the discretely heated wall with subsequent movement toward the isothermal wall.

A similarly good level of qualitative agreement is seen between the interferometric data and the predicted isotherms for single heater locations of $s/H = 0.5$ and 0.2, seen in Figs. 3 and 4, respectively. By contrast with the $s/H = 0.8$ result, there exists a large region of isothermal fluid in the portion of the cavity below the heat source for smaller values of s/H. This isothermal region is nearly stagnant, as is demonstrated by the predicted steam function contours. As the heat source rises to positions higher in the cavity, the same general circular motion described above is observed, with the exception that less of the cavity is buoyancy affected; the primary recirculation eddy generally occupies only the portion of the cavity above the leading edge of the heater. The discrete heating studied here thus results in recirculation cells the size and location of which vary with heater location. As will be demonstrated in a section to follow, the radical difference in the extent of the recirculating flow eddy will have a significant effect on the heat transfer from the heated strip.

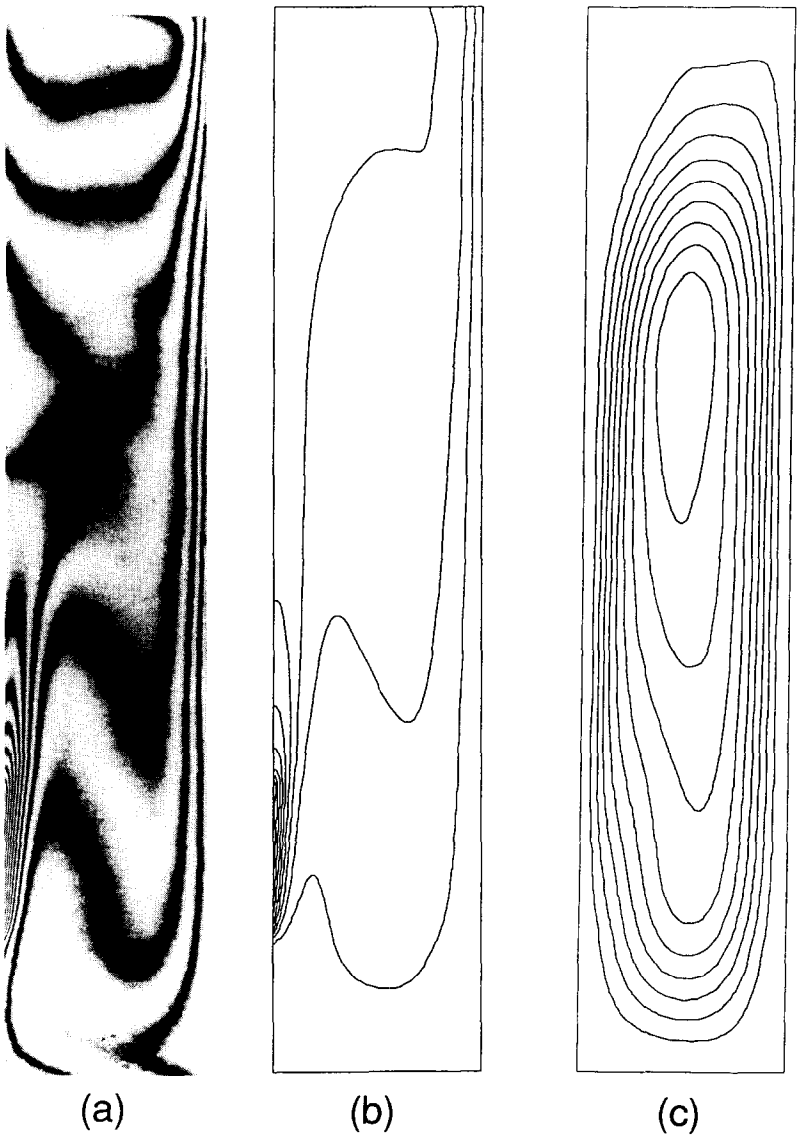

FIG. 2. Mach–Zehnder interferogram and predicted temperature field and flow structure for single heater configuration, $s/H = 0.8$, $H/W = 5$, $Gr = 5.12(10^5)$.

The local Nusselt numbers along the heated strips, calculated from the Mach–Zehnder interferograms in Figs. 2–4, are shown in Fig. 5 with the results of the theoretical predictions. The plotted symbols reflect the results of three experiments with the single heater locations of $s/H = 0.2$, 0.5, and 0.8, for nearly the same Grashof number. The growth of a thermal boundary layer along the heater observed in the interferograms previously are more clearly evident in Fig. 5. A relatively high heat transfer coefficient exists at the leading edge of the heater regardless of its position in the cavity, with decaying Nusselt number thereafter. The local heat transfer varies in magnitude by a factor of two over the length of each heater, indicating significant surface temperature gradients there.

The model predictions show excellent agreement with the experimental data in Fig. 5, the maximum deviation being only 8%. It is reasoned that conjugate heat transfer from the heat source to the insulating substrate resulted in the slight deviations from analytical predictions. Although the polystyrene insulation was used to prevent conjugate heat losses from the experimental apparatus, redistribution of the Ohmic heat flux still occurs to some extent. This results in an averaging effect on the local heat transfer distributions, and thus causes the smearing in Nusselt number with changes in position y/H on the heat source, as seen in Fig. 5.

The predicted and experimentally determined local Nusselt number data seen in Fig. 5 reveal generally increasing heat transfer coefficients for increasing s/H. The variation in Nusselt number is slight but noticeable, the difference in Nu being approximately 10% at the leading edge for the $s/H = 0.2$ and 0.8 extremes in heater placement studied. As alluded to in the foregoing, the increasing heat transfer with increasing s/H

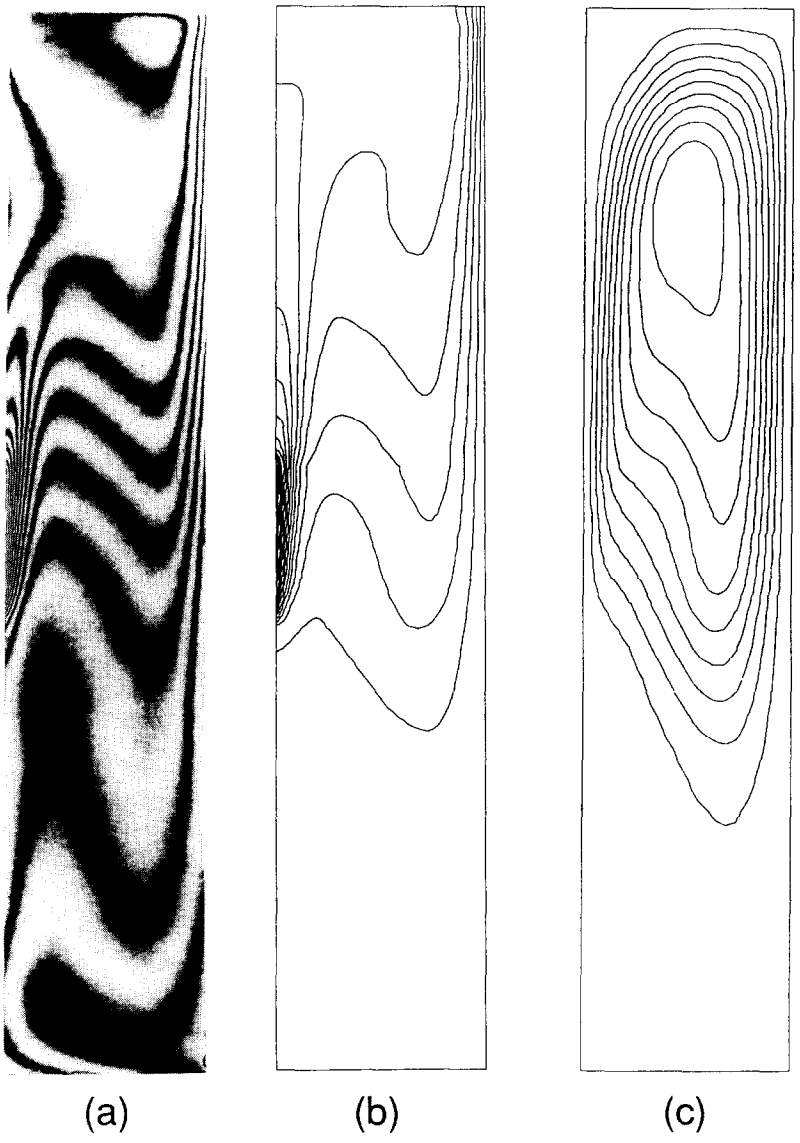

FIG. 3. Mach–Zehnder interferogram and predicted temperature field and flow structure for single heater configuration, $s/H = 0.5$, $H/W = 5$, $Gr = 5.16(10^5)$.

may be explained in terms of the growth of the primary recirculating eddy as the heater is moved down along the discretely heated wall. A larger portion of the enclosure is affected by the buoyancy-driven flow when the heater occupies a position lower in the cavity. The larger recirculation cell indicates that more of the cooled wall is thermally active. This is illustrated by the predictions of the maximum stream function, Ψ_{max}, versus heater location, s/H, corresponding to the conditions of Fig. 5. The maximum stream function is reflective of the intensity of mass flow in the primary recirculation cell. The predicted maximum normalized stream function for the $s/H = 0.2$, 0.5, and 0.8 cases with $Gr = 1.2(10^6)$ were found to be 23.2, 53.8, and 77.8, respectively. These data suggest that the increase in local Nusselt number observed in Fig. 5 is due to the increased intensity of natural convection flow in the enclosure, reflected by increasing Ψ_{max}. There is a threefold increase in the dimensionless mass flow rate in the recirculation cell. As observed in the stream function contours and Ψ_{max} data, the increased mass movement observed in the $s/H = 0.8$ configuration causes more interaction with the cooled isothermal wall. The fluid approaching the heat source is thus at a lower temperature than for the higher heater locations, which results in more effective cooling of the concentrated heat source at the heated wall.

The local heat transfer profiles were correlated using an equation suggested by the analytical solution for free convection from a vertical plate with a uniform heat flux imposed at the surface [17]

$$Nu_{y'} = B\,Gr_{y'}^{n}. \tag{9}$$

The coordinate y' is measured from the leading edge of the heater. Describing the local heat transfer with

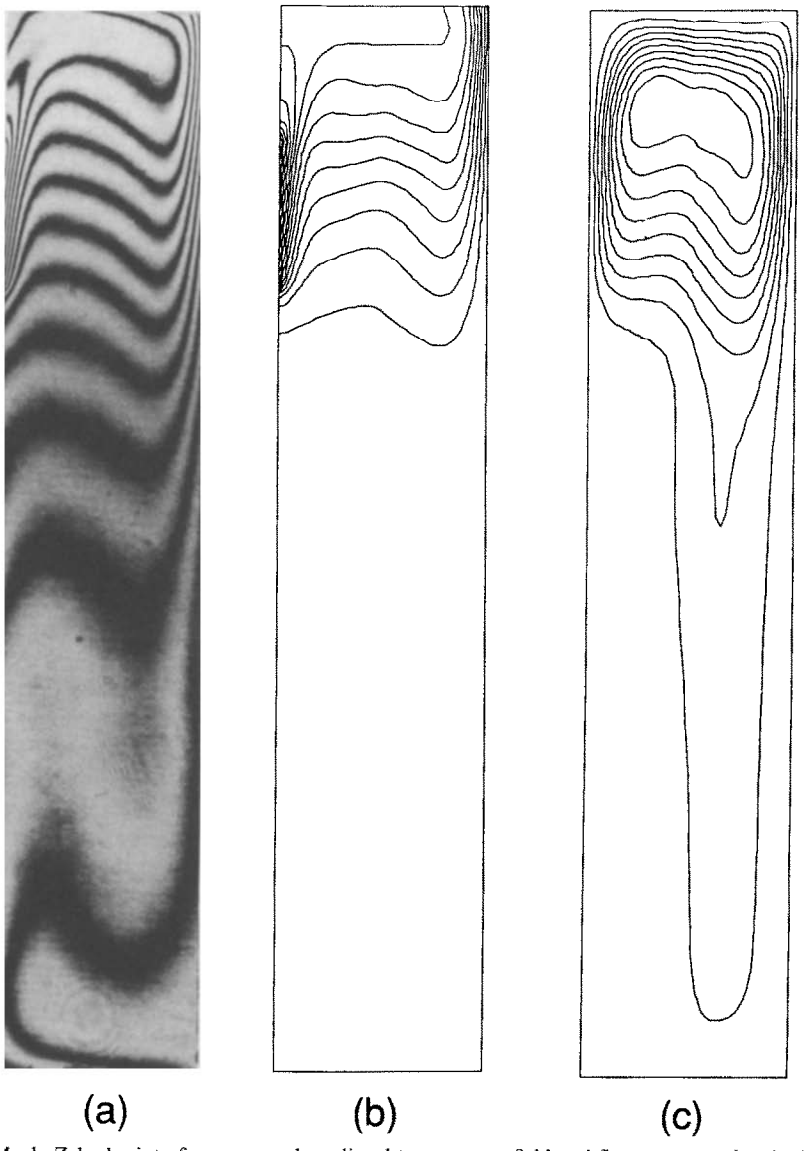

FIG. 4. Mach–Zehnder interferogram and predicted temperature field and flow structure for single heater configuration, $s/H = 0.2$, $H/W = 5$, $Gr = 3.10(10^5)$.

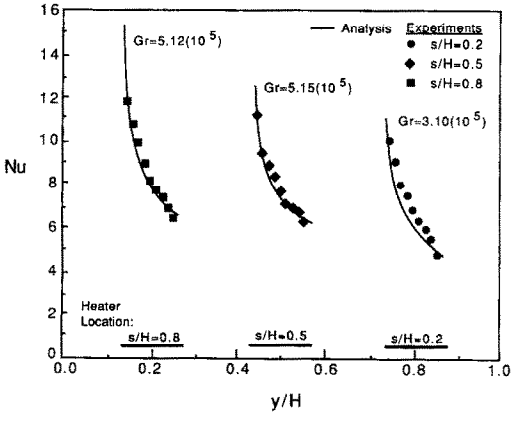

FIG. 5. Local Nusselt number distributions and model predictions for single heater configuration, enclosure aspect ratio $H/W = 5$.

equation (9), the coefficients and exponents for various heater locations and, for comparison, the exact solution for the isolated vertical plate for $Pr = 0.71$ [17] are shown in Table 1. The coefficients and exponents were obtained from least-squares regression fits of the predictions over a range of Grashof numbers, with an average error of 2.0%.

The correlations presented in Table 1 illustrate several points. The $s/H = 0.8$ single heat source system exhibits slightly higher heat transfer coefficient only at the leading edge of the heater ($Gr_{y'} \to 0$) than the vertical plate solution, with lower heat transfer coefficient over the remainder of the surface. The $s/H = 0.5$ and 0.2 configurations both yield lower local Nusselt number over the entire heater face. The decay in local heat transfer coefficient along the discrete heaters is somewhat higher than for the isolated

Table 1. Coefficients and exponents for correlation equation (9), single and dual heater configurations, enclosure aspect ratio $H/W = 5$

S/H	B	n
Vertical plate [17]	0.495	0.20
0.2	0.438	0.193
0.5	0.454	0.199
0.8	0.526	0.192

vertical plate, indicated by the smaller exponent, n. This may be due to interaction with the downward-directed flow along the isothermal wall.

Comparisons between the predicted average Nusselt number and the experimental results calculated from the local data according to equation (6) are shown in Fig. 6. Excellent agreement exists between prediction and experiment. The average and maximum error between prediction and experimental data are 5.9 and 7.9%, respectively. For all single heater locations the predicted average Nusselt number increased approximately with $Gr^{1/5}$ over the Grashof number range $10^4 \leqslant Gr \leqslant 10^7$. The predicted data may be correlated very well with an expression of the form

$$\overline{Nu} = A\,Gr^m \tag{10}$$

where for $s/H = 0.8$, 0.5, and 0.2 the regression values for A are 0.59, 0.61, and 0.39 with corresponding exponents $m = 0.20$, 0.19, and 0.22, respectively. Also shown in Fig. 6 is the analytical solution for free convection in air ($Pr = 0.71$) from a vertical plate of length L [17], given by $\overline{Nu} = 0.594Gr^{1/5}$. The predicted average heat transfer coefficient for the discretely heated enclosure is always lower than the free vertical plate result in the Grashof number range shown. It appears that the average heat transfer characteristics of a single discrete heat source approach that of the free vertical plate as its location moves toward the bottom of the enclosure (s/H is increased); the correlated $s/H = 0.8$ predictions are less than 2% below the vertical plate result.

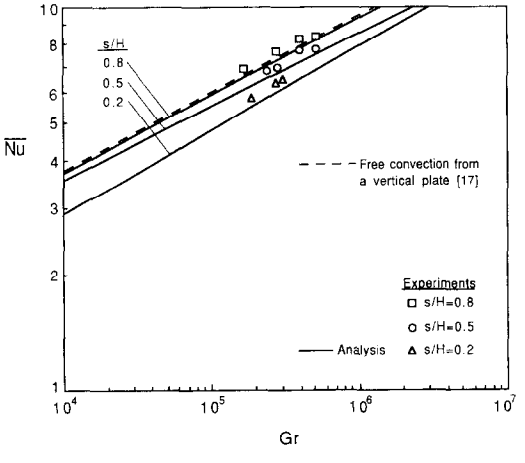

FIG. 6. Average Nusselt number dependence on Grashof number for single heat source configuration, $H/W = 5$.

The heat transfer coefficient has been seen to rise with increasing s/H; for a given Grashof number the maximum Nusselt number occurs for $s/H = 0.8$. An approximate 7% reduction in average Nusselt number was observed when the heat source was moved from $s/H = 0.5$ to 0.2, and a 17% reduction when moved from $s/H = 0.8$ to 0.2. Previous investigations have revealed that the maximum heat transfer occurs for a heater location near $s/H = 0.5$ for Grashof numbers significantly lower than those studied here ($Gr_H \leqslant 1.43(10^5)$ in the study by Chu *et al.* compared to $Gr_H \geqslant 5.36(10^8)$ in this study) [3, 4]. Chu *et al.* also showed that the heater location corresponding to optimum heat transfer is Grashof number dependent; the maximum Nusselt number was found at higher s/H for increasing Grashof number. The slight differences in slope of the predicted $\overline{Nu}$–Gr distribution shown in Fig. 6 corroborate this finding. If one extrapolates the predictions for the average Nusselt number to $Gr < 10^4$ it is seen that a maximum in the $\overline{Nu}$ data will be found for the $s/H \approx 0.5$ configuration. Indeed, using the analytical model developed in this study, the Nusselt number maximum for $s/H = 0.5$ at low Gr predicted by Chu *et al.* [3] was duplicated. Conditions identical to those previously studied were simulated and the differences in the predicted average heat transfer from the two investigations were found to be less than 10%. The difference is attributed to the more refined 60×60 grid used in this study relative to the 20×20 node distribution used in the previous work.

Interestingly, the maximum predicted stream function followed the same trend as the average Nusselt number just described. Higher Ψ_{max} was found to occur at $s/H \approx 0.8$ in the high Gr range, and at $s/H \approx 0.5$ in the low Gr range. This supports the observation made previously that the heat transfer is strongly dependent on the intensity of the buoyancy-driven flow in the cavity as reflected by the value of Ψ_{max}.

DUAL HEAT SOURCE CONFIGURATION

Two heat sources were placed in the cavity and studied experimentally for Case 1 ($s/H = 0.5$ and 0.8) and Case 2 ($s/H = 0.2$ and 0.5) for enclosure aspect ratios of $H/W = 4$, 5, and 6. Despite identical electrical power delivered to both heater strips, the convective heat transfer from the two heat sources was different due to unequal convective and radiative losses. This difference in convective heat flux for the two heaters was found to be as high as a factor of two for the Case 2 configuration, where the top heater ($s/H = 0.2$) had substantially lower heat transfer coefficient than the bottom heater ($s/H = 0.5$). This resulted in higher temperatures and associated higher radiative and conductive losses at the top. The difference in convective heat flux imposed at the two heaters

for the Case 1 configuration never exceeded 10%. The Grashof number describing the dual heat source experiments was thus based on the average convective heat flux for the two heaters. The thermal and flow structure for the dual heat source configuration Case 2 with enclosure aspect ratios $H/W = 5$ and 6 were qualitatively similar to the single heat source at $s/H = 0.5$. Thermal boundary layers formed along each heat source and a single recirculation cell occupied the upper half of the cavity. However, for Case 2 and $H/W = 4$ the complex flow structure shown in Fig. 7 was observed. Small recirculation zones develop in the middle of the channel at the top of the enclosure. The structure of the temperature field is also seen to be quite complex. These complex flow and thermal patterns were not observed in the higher aspect ratio (more slender) enclosure cases. The complexity in the flow and thermal structures observed in Fig. 7 may be caused by the reduced interaction between the hydrodynamic boundary layers on the heated and cooled walls for the higher wall spacing, $H/W = 4$ enclosure.

All aspect ratios for the dual heater Case 1 configuration ($s/H = 0.5$ and 0.8) exhibited the same general flow patterns as the single heater system with $s/H = 0.8$ (see Fig. 8). Thermal boundary layers started at the bottom of each heat source and grew as the fluid rose along the heated wall due to buoyancy. There was an interruption in the thermal boundary layer due to the adiabatic section between the two heat sources and at the top of the upper heat source. This interrupted boundary layer due to the discrete heating will be shown to influence the local heat transfer characteristics of the second heat source in a significant way. A thermal boundary layer thicker than that observed along each discrete heat source was seen to form along the isothermal wall as the fluid was

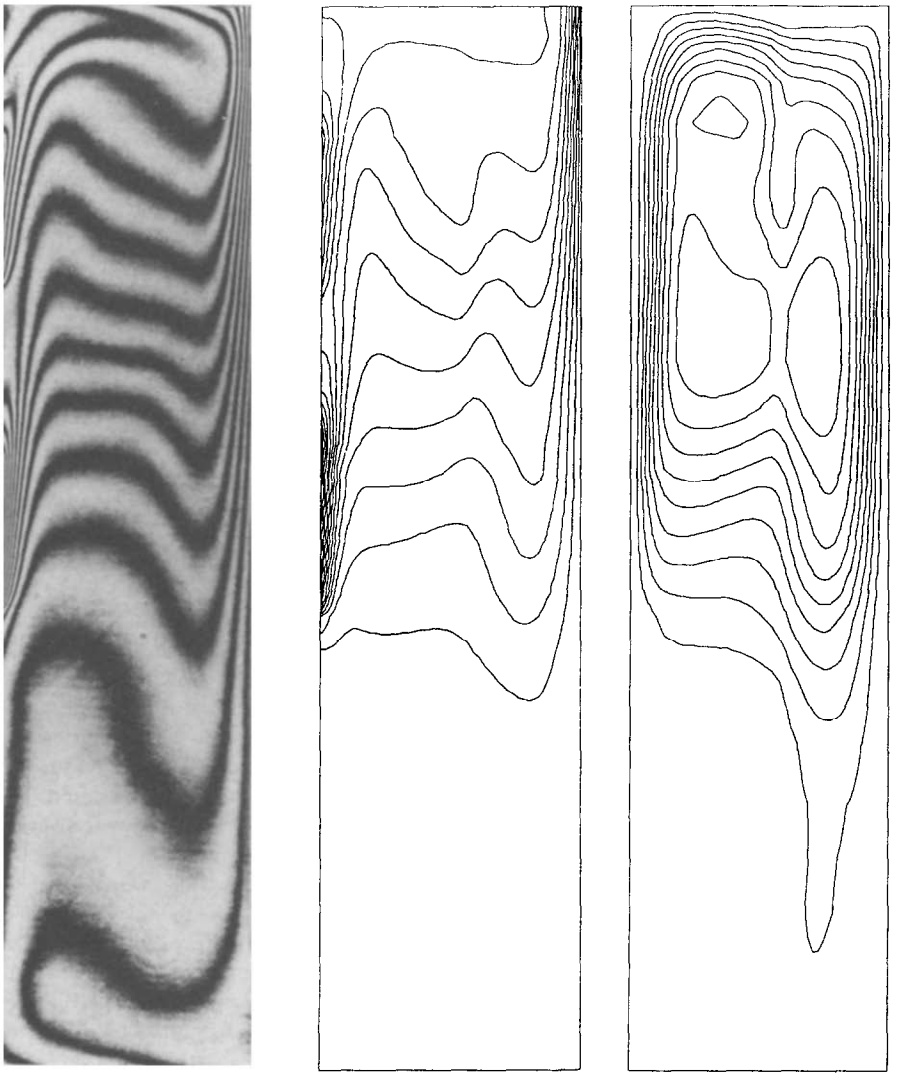

FIG. 7. Mach–Zehnder interferogram and predicted temperature field and flow structure for dual heater configuration Case 2 ($s/H = 0.2$ and 0.5), $H/W = 4$, $Gr = 3.43(10^5)$.

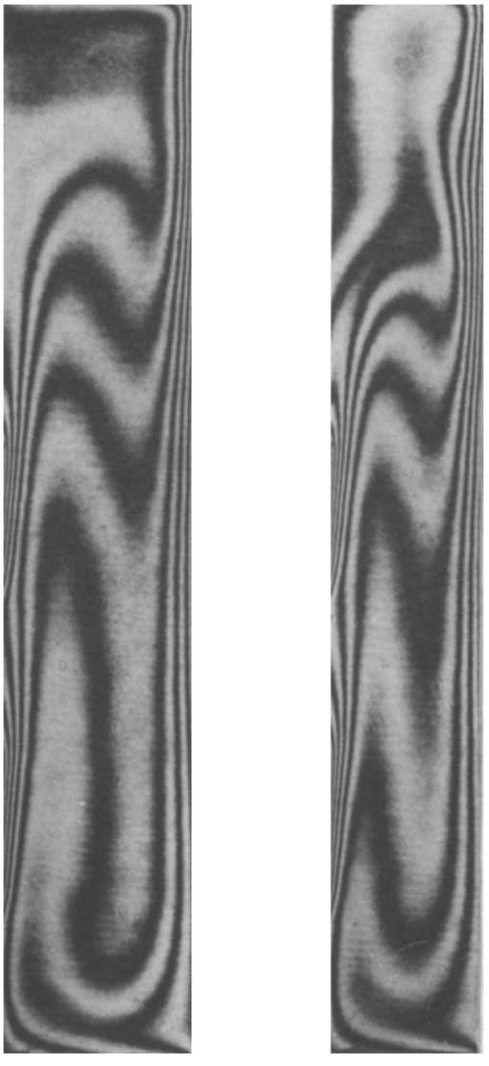

FIG. 8. Comparison of temperature distributions for dual heater configuration Case 1 ($s/H = 0.5$ and 0.8), $Gr = 3.22(10^5)$: (a) $H/W = 5$; (b) $H/W = 6$.

cooled during its descent. The effect of cavity aspect ratio is seen for Cases 1 and 2 at the same nominal Grashof number in Figs. 8 and 9. The figures show that the zone of stably-stratified, stagnant fluid in the center portion of the enclosure decreases in width as the aspect ratio increases. This is especially evident in Fig. 9 for Case 2 ($s/H = 0.2$ and 0.5), where the thermal (and presumably the hydrodynamic) boundary layers interact more significantly in slender cavities. Indeed, predictions for aspect ratios higher than $H/W = 6$ (more slender cavities) reveal that viscous effects begin to dominate as the boundary layers along the two walls merge and the heat transfer decreases [18].

The predicted and experimentally-determined local Nusselt numbers for two dual heater configuration experiments, Cases 1 and 2, are shown in Fig. 10 for $Gr = 3.15(10^5)$ and $3.30(10^5)$, respectively. The results are for an enclosure aspect ratio $H/W = 5$. Again, the effect of the thermal boundary layer growing along each heater is evident; the local heat transfer coefficient starts relatively high at the leading edge of each heater and drops monotonically. Case 1 shows that the heat transfer at the leading edge of the upper heater ($s/H = 0.5$) is actually higher than the local Nusselt number at the trailing edge of the lower heater. The rise in heat transfer is a consequence of the interruption of the thermal boundary layer between the discrete heat sources illustrated in Figs. 7–9. This enhancement phenomenon due to the interrupted boundary layer is not observed in the $s/H = 0.2$, 0.5 (Case 2) dual heater configuration. As was the case with the single heater enclosure, generally more effective cooling is observed when the discrete heating occurs at the bottom of the cavity. This has been explained in terms of the more intense buoyancy-driven recirculation cell which occupies a larger portion of the enclosure. It is also observed by the data of Fig. 10 that heat transfer from the bottom heat source in a two-heater enclosure is affected only marginally by the presence of a heater above.

The model predictions shown in Fig. 10 agree well with the experimental data. The maximum error in Nusselt number is only 8%. The predicted local Nusselt number profiles exhibit a nearly power-law decreasing distribution and the experimental data were again smeared. Once again, this is believed to be caused by the conjugate effects in the insulating substrate.

A plot of the comparison between the experimental and predicted average Nusselt numbers for an aspect ratio of $H/W = 5$ can be seen in Fig. 11. The analytical average Nusselt numbers for heater locations of $s/H = 0.5$ and 0.8 were within 8% of the experimental Nusselt numbers for cavity aspect ratios of $H/W = 4$, 5, and 6. The analytical average Nusselt number (assuming identical heat flux imposed at both heaters) for the heater location $s/H = 0.2$ varied by nearly 30% from the experimental results. This is explained by the different radiation heat transfer and conduction heat loss from the top and bottom heat sources. Although equal electrical energy was supplied to both heaters, the comparatively low heat transfer coefficient at $s/H = 0.2$ yielded higher temperatures there. The result was higher radiative and conductive heat loss at the top heater. A radiation analysis was performed by dividing the enclosure into 14 surfaces, nine along the discretely heated wall, two each on both the top and bottom walls, and a single surface along the isothermal wall. The temperatures of each of these surfaces were estimated from the Mach–Zehnder interferograms, and the emissivities specific to each surface material were taken from the literature [19]. Assuming diffuse gray surface behavior, standard techniques [20] were employed for calculating the net radiation heat transfer from each surface in the enclosure. The results of the radiation analysis revealed that the ratio of radiative to convective heat flux at the heater sur-

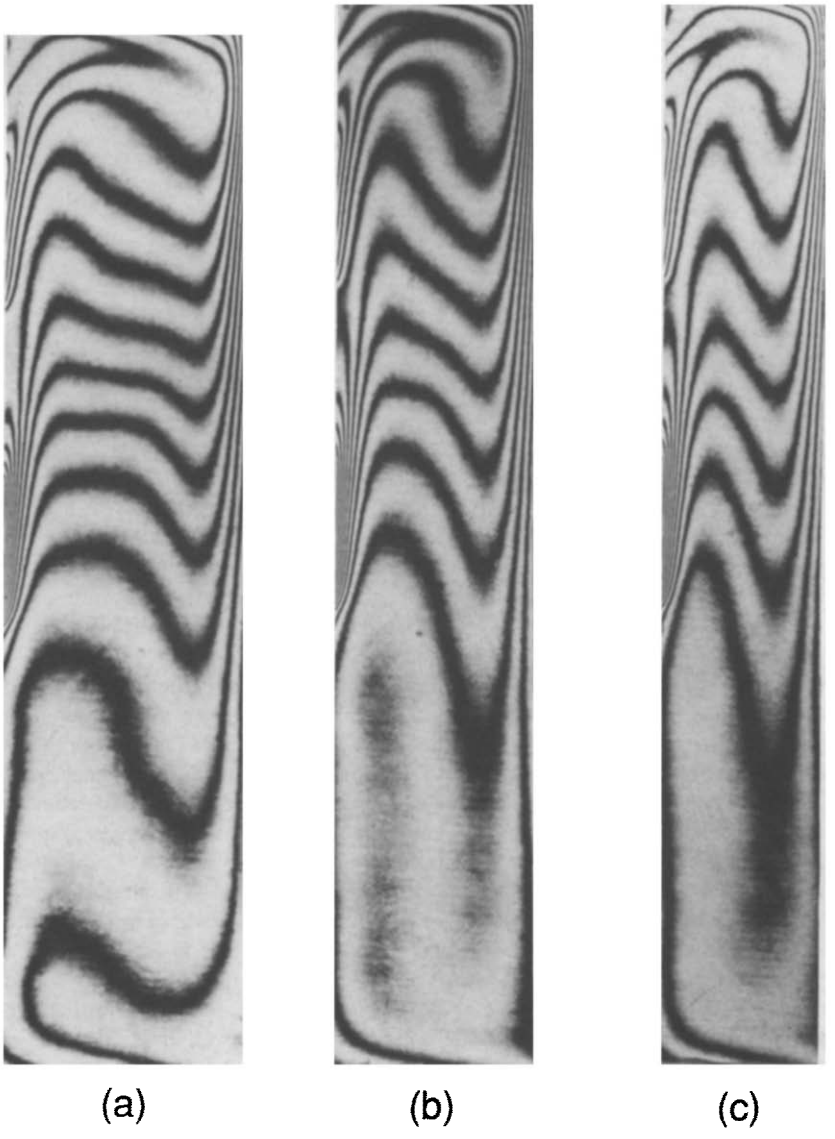

FIG. 9. Comparison of temperature distributions for dual heater configuration Case 2 ($s/H = 0.2$ and 0.5), $Gr = 3.11(10^5)$: (a) $H/W = 4$; (b) $H/W = 5$; (c) $H/W = 6$.

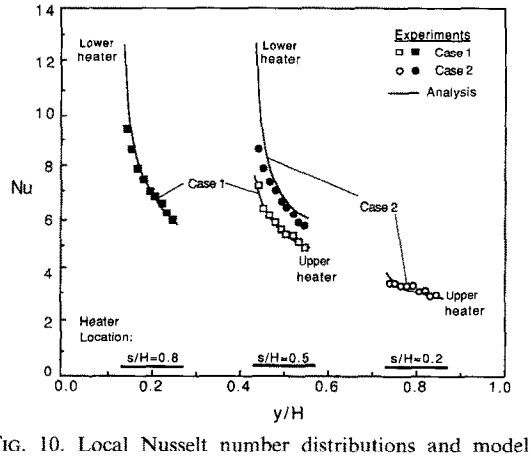

FIG. 10. Local Nusselt number distributions and model predictions for dual heater configuration, enclosure aspect ratio $H/W = 5$: Case 1, $Gr = 3.15(10^5)$; Case 2, $Gr = 3.30(10^5)$.

faces for the Case 2 configuration were in the range 0.60–0.71 for $s/H = 0.2$, and 0.28–0.35 for $s/H = 0.5$. This ratio for the Case 1 system was found to vary from 0.31 to 0.36 for $s/H = 0.5$, and 0.23 to 0.31 for $s/H = 0.8$. In dual heater theoretical simulations presented previously in this study, identical heat flux (determined from the average of the experimental data) was imposed at the two heat sources. By imposing the different convective heat fluxes determined for each heater from the interferograms in the thermal boundary condition of the theoretical simulations the predicted average Nusselt number came within 7% of the experimental average Nusselt numbers for the Case 2 configuration and for aspect ratios $H/W = 4$, 5, and 6. The Case 2 dual heat source configuration ($s/H = 0.2$ and 0.5) was particularly vulnerable to the radiation and conduction losses because of its characteristically low heat transfer, as was illus-

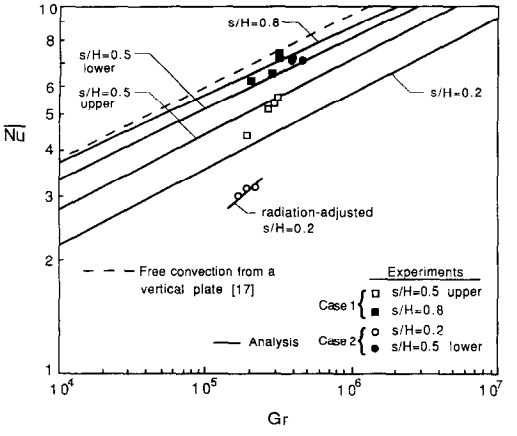

FIG. 11. Average Nusselt number dependence on Grashof number for dual heat source configuration, $H/W = 5$.

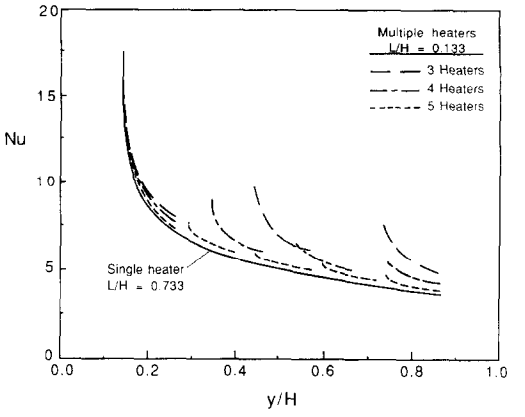

FIG. 12. Predicted local Nusselt number profiles for three, four, and five heat sources with continuous heating comparison, $Gr = 1.2(10^6)$.

trated in Fig. 10. The simulation results with radiation adjustment to the heat flux imposed at each heater are also shown in Fig. 11, and similar results were obtained for aspect ratios of $H/W = 4$ and 6 [18]. The Case 1 predictions were always produced using identical heat fluxes imposed at both heat sources.

The same observations made for the local heat transfer behavior made relative to the data of Fig. 10 may be stated for the average Nusselt number data of Fig. 11. Generally speaking, the top heater suffers from lower heat transfer coefficient than the bottom heater. For aspect ratios of $H/W = 4$, 5, and 6 the average Nusselt number for the top heater is 20–40% higher than the bottom heater in the dual heat source configuration, depending on Grashof number. This is true for either Case 1 or Case 2 dual heater system.

Within the range analyzed in this study ($H/W = 2$–8), and all other geometric and system parameters remaining constant, changes in aspect ratio were observed to have only a minor effect on the heat transfer characteristics of the discretely-heated enclosure [18].

MULTIPLE HEAT SOURCE CONFIGURATION

The analytical models were in good agreement with the experimental simulations for single and dual heater configurations for a wide range of aspect ratio, heater location, and Grashof number. This provided confidence in the extension of the theoretical model to multiple heat source configurations. Discrete, uniform heat flux sources were placed in varying numbers along the heated wall. An enclosure of aspect ratio $H/W = 5$ was used in all multiple heater simulations. The top and bottom heaters for all configurations with three or more heat sources were at fixed locations of $s/H = 0.2$ and 0.8, respectively. This left an unheated section of $L/H = 0.133$ at the top and bottom of the enclosure. Three, four, or five heat sources of length $L/H = 0.133$ were equally spaced between the fixed adiabatic sections at the top and bottom. Predictions for a continuously heated wall were also made, for which the heater length was $L/H = 0.733$ with adiabatic sections at the cavity top and bottom identical in length to the discrete heat source systems. The Grashof number for all multiple heater configurations was studied in the range $10^4 \leqslant Gr \leqslant 5(10^6)$. The continuously heated wall predictions were made with the same imposed heating rate as the discrete heater solutions. To provide a basis for appropriate comparison to the discrete heat source predictions, the same characteristic length L was used to define the Grashof and Nusselt numbers for the single continuous heater ($L/H = 0.733$) case.

The predicted local Nusselt number profiles for three, four, and five heat sources of identical length, $L/H = 0.133$, are shown in Fig. 12 for $Gr = 1.2(10^6)$. Also shown for comparison is the single continuous heater ($L/H = 0.733$) prediction for the same imposed heat flux. It may be observed that the single continuous heater yielded generally lower local heat transfer coefficient than the multiple heat sources. As the number of heat sources was increased the local heat transfer for heaters at corresponding s/H locations decreased. This illustrates the influence of the thermal wake from heat sources below. The extent of decrease in heat transfer depends upon the heater location. The heaters with fewer heat sources below them exhibit higher heat transfer because of reduced prior boundary layer growth. In fact, the local heat transfer for the heat source at $s/H = 0.8$ is only marginally different for all multiple heater configurations studied including the continuously heated wall.

The predicted average Nusselt number was calculated from the local heat transfer data for the multiple heater simulations. The dependence of the average Nusselt number on Grashof number in the range $10^4 \leqslant Gr \leqslant 5(10^6)$ was correlated using an expression of the form

$$\overline{Nu}_i = C_i\, Gr^{0.215} \tag{11}$$

where $\overline{Nu}_i$ is the average Nusselt number for heat source i ($i = 1, 2, 3, \ldots$, numbering beginning at the top of the enclosure), and C_i the regression coefficient

Table 2. Coefficients for equation (11) derived from the analytical study of various numbers of heat sources for an aspect ratio of $H/W = 5$

Three heat sources $L_{uh}/H = 0.1667$ $(L+L_{uh})/L = 2.25$			Four heat sources $L_{uh}/H = 0.0667$ $(L+L_{uh})/L = 1.50$			Five heat sources $L_{uh}/H = 0.01667$ $(L+L_{uh})/L = 1.125$		
Heater	s/H	C_i	Heater	s/H	C_i	Heater	s/H	C_i
1	0.2	0.272	1	0.2	0.228	1	0.20	0.204
2	0.5	0.339	2	0.4	0.267	2	0.35	0.237
3	0.8	0.453	3	0.6	0.330	3	0.50	0.263
			4	0.8	0.427	4	0.65	0.318
						5	0.80	0.425

corresponding to heater i. Table 2 contains the coefficients C_i for use in the average Nusselt number correlation of equation (11) for three, four, and five heat sources for an enclosure of aspect ratio $H/W = 5$. In reality the exponent of Gr varied between 0.199 and 0.218 with associated slight changes in the coefficient C_i. However, an average value of 0.215 with the coefficients shown reflects the Grashof number dependence in the prescribed range with a maximum error of 3%.

The table shows that the heat sources in the lower part of the cavity exhibit the highest average Nusselt number, this being a result of the thinner thermal boundary layer there. Keyhani *et al.* [6] found that the ratio of the average Nusselt number of the second heater up to that of the bottom heaters in a ten-heater, $H/W = 16.5$ system was 0.79 for $(L+L_{uh})/L = 2$. The correlations of Table 2 indicate that for $H/W = 5$, this ratio for the bottom two heaters has a numerical value of 0.76, and is nearly independent of both L_{uh}/L and the total number of discrete heaters in the enclosure. However, it is observed that the ratio of average heat transfer coefficient between the upper and lower heater of subsequent adjacent heater pairs increases with increasing total number of heaters in the enclosure and corresponding decrease in L_{uh}/H. This is at variance with the dual, flush, in-line heater free convection results of ref. [21], where the difference between heat transfer coefficient for the top and bottom heaters was found to diminish with increasing separation distance. This may be explained by the different flow characteristics of the enclosure flow for increasing discrete heat sources of this study and the free convective flow and heat transfer of ref. [21].

A comparison of the average Nusselt number for the bottom heater in the five-heater enclosure, $H/W = 5$, from this study with that of the corresponding bottom heater in the ten-heater enclosure, $H/W = 16.5$, of Keyhani *et al.* [6] may be made. The correlation of experimental data given in ref. [6] is $\overline{Nu}_W = 0.345 Ra_W^{0.242}$. The corresponding correlation for the five-heater enclosure of this study using the cavity width as the characteristic length in the Nusselt and Rayleigh number is $\overline{Nu}_W = 0.538 Ra_W^{0.215}$. The two correlations agree to within 9% over the Rayleigh number range $10^4 \leqslant Ra_W \leqslant 10^7$.

Table 2 also indicates that the average heat transfer coefficient for heaters at identical locations in the enclosure decreases as the number of heaters increases. Calculations show that all heaters in the multiple heat source configurations exhibit lower average heat transfer coefficient than that for free convection from an isolated vertical plate of the same heater length, L, given by $\overline{Nu} = 0.594 Gr^{1/5}$. This is similar to that predicted for the single and dual heater configurations illustrated in Figs. 6 and 11. The comparisons made in the foregoing paragraphs relative to Table 2 illustrate the enormous impact of the thermal wake from heat sources below on those above. The heater location and the number of heaters within the enclosure affect the heat transfer in a significant way for a given Grashof number.

CONCLUSIONS

Natural convection in a discretely heated enclosure for single and multiple heater locations has been investigated experimentally and theoretically. Experiments were performed with single and dual heat source configurations. Mach–Zehnder interferometry was used to visualize the temperature field within the enclosure and to determine the local heat transfer characteristics of the discrete heat sources. The partial differential equations governing the conservation of mass, momentum and energy were solved for the system using a control volume-based finite difference method. After validation of the model by comparison with experimental data, predictions were made for a broader range of problem parameters, and correlations were developed for the local and average Nusselt number.

For the single heat source configuration the heater location of $s/H = 0.8$ resulted in 7 and 17% higher average heat transfer coefficients, respectively, than the $s/H = 0.5$ and 0.2 locations. The Grashof number was studied in the range from $1.6(10^5)$ to $5.2(10^5)$ experimentally, and $1.0(10^4)$ to $5.0(10^6)$ numerically for a single aspect ratio of $H/W = 5$. This study corroborates the observation of previous work that the heat source location corresponding to maximum heat transfer was also a function of Grashof number. This phenomenon was explained in terms of the intensity of the buoyancy-driven flow in the enclosure, quant-

ified by the stream function at the primary recirculation eddy center.

The Case 1 heater location ($s/H = 0.5$ and 0.8) resulted in the highest heat transfer coefficient for the dual heater configurations. The Grashof number dependence for the two heater system was studied in the range from $1.4(10^5)$ to $4.7(10^5)$ experimentally and numerically from $1.0(10^4)$ to $5.0(10^6)$ for enclosure aspect ratios of $H/W = 4$, 5, and 6. The thermal wake of the bottom heat source was seen to significantly affect the transport from the upper heater, resulting in a reduction in $\overline{Nu}$ by 20–40%, depending on Gr. The lower heat source was influenced only marginally by the presence of a heater above. This observation was also found for numerical predictions of multiple heat sources in the enclosure.

Acknowledgements—This work was supported by the U.S. National Science Foundation under grant CBT-8552493. The computational work was made possible by a computer equipment donation from the Digital Equipment Corporation.

REFERENCES

1. F. P. Incropera (Editor), Research needs in electronic cooling, Proc. workshop sponsored by the National Science Foundation and Purdue University, Andover, Massachusetts, (1986).
2. R. J. Moffatt and A. Ortega, Direct air-cooling of electronic equipment. In *Advances in Thermal Modeling of Electronic Components and Systems* (Edited by A. Bar-Cohen and A. D. Kraus), Vol. 1. Hemisphere, New York (1988).
3. H. H. S. Chu, S. W. Churchill and C. V. S. Patterson, The effects of heater size, location, aspect ratio, and boundary conditions on two-dimensional, laminar natural convection in rectangular channels, *ASME J. Heat Transfer* **98,** 194–201 (1976).
4. B. L. Turner and R. D. Flack, The experimental measurement of natural convective heat transfer in rectangular enclosures with concentrated energy sources, *ASME J. Heat Transfer* **102,** 236–241 (1980).
5. R. D. Flack and B. L. Turner, Heat transfer correlations for use in naturally cooled enclosures with high-power integrated circuits, *IEEE Trans. Components Hybrids Mfg Technol.* **CHMT-33,** 449–452 (1980).
6. M. Keyhani, V. Prasad and R. Cox, An experimental study of natural convection in a vertical cavity with discrete heat sources, *ASME J. Heat Transfer* **110,** 616–624 (1988).
7. M. Keyhani, V. Prasad, R. Shen and T. T. Wong, Free convection heat transfer from discrete heat sources in a vertical cavity. In *Natural and Mixed Convection in Electronic Equipment Cooling* (Edited by R. A. Wirtz), pp. 12–24. ASME, New York (1988).
8. R. Shen, V. Prasad and M. Keyhani, Effect of aspect ratio and size of heat source on free convection in a discretely heated vertical cavity. In *Numerical Simulation of Convection in Electronic Equipment Cooling* (Edited by A. Ortega and D. Agonafer), pp. 45–54. ASME, New York (1989).
9. M. D. Kelleher, R. H. Knock and K. T. Yang, Laminar natural convection in a rectangular enclosure due to a heated protrusion on one vertical wall—Part I: experimental investigation, *Proc. 2nd ASME/JSME Thermal Engng Joint Conf.*, Vol. 2, pp. 169–177. ASME, New York (1987).
10. Y. Joshi, M. D. Kelleher and T. J. Benedict, Natural convection immersion cooling of an array of simulated electronic components in an enclosure filled with dielectric fluid, *Proc. Int. Exp. Heat Transfer Conf.*, Yugoslavia (1988).
11. L. Chen, M. Keyhani and D. R. Pitts, An experimental study of natural convection heat transfer in a rectangular enclosure with protruding heaters, *Proc. Natn. Heat Transfer Conf.*, Vol. 96, Part 2, pp. 125–133. ASME, New York (1988).
12. J. J. Lee, K. V. Liu, K. T. Yang and M. D. Kelleher, Laminar natural convection in a rectangular enclosure due to a heated protrusion on one vertical wall—Part II: numerical simulations, *Proc. 2nd ASME/JSME Thermal Engng Joint Conf.*, Vol. 2, pp. 179–185. ASME, New York (1987).
13. W. Hauf and U. Grigull, Optical methods in heat transfer. In *Advances in Heat Transfer* (Edited by J. P. Hartnett and T. F. Irvine, Jr.), Vol. 6, pp. 276–277. Academic Press, New York (1970).
14. S. J. Kline and F. A. McClintock, Describing uncertainties in single-sample experiments, *Mech. Engng* 3–12 (January 1953).
15. S. V. Patankar, *Numerical Heat Transfer and Fluid Flow*. Hemisphere, Washington, DC (1980).
16. E. R. G. Eckert and W. O. Carlson, Natural convection in an air layer enclosed between two vertical plates with different temperatures, *Int. J. Heat Mass Transfer* **2,** 106–120 (1961).
17. E. M. Sparrow and J. L. Gregg, Laminar free convection from a vertical plate with uniform surface heat flux, *Trans. ASME* **78,** 435–440 (1956).
18. M. L. Chadwick, Natural convection from two-dimensional discrete heat sources in a rectangular enclosure with and without venting, M.S. Thesis, Brigham Young University, December (1989).
19. F. P. Incropera and D. P. DeWitt, *Introduction to Heat Transfer*, 2nd Edn. Wiley, New York (1990).
20. R. Siegel and J. R. Howell, *Thermal Radiation Heat Transfer*, 2nd Edn. Hemisphere, Washington, DC (1981).
21. K. A. Park and A. E. Bergles, Natural convection heat transfer characteristics of simulated microelectronic chips, *ASME J. Heat Transfer* **109,** 90–96 (1987).

CONVECTION NATURELLE AUTOUR DE DEUX SOURCES DISCRETES BIDIMENSIONNELLES DANS UNE CAVITE RECTANGULAIRE

Résumé—On étudie expérimentalement et théoriquement la convection naturelle dans une cavité avec chauffage discrétisé pour des configurations à chauffoir unique ou multiple. L'interférométrie Mach–Zehnder est utilisée pour visualiser le champ de température dans la cavité et pour déterminer les caractéristiques locales et moyennes du transfert de chaleur. Les équations aux dérivées partielles qui gouvernent la convection de la masse, de la quantité de mouvement et de l'énergie, sont résoluent numériquement. Les résultats montrent que pour la configuration à une seule source, la position du chauffoir très proche du plancher de la cavité conduit au transfert thermique le plus élevé, dans le domaine des grands nombres de Grashof. Néanmoins est confirmée l'observation d'un travail antérieur selon laquelle la position de la source correspondant au maximum du transfert thermique est fonction du nombre de Grashof. Plusieurs chauffoirs logés près de la base de la cavité donnent aussi le plus fort transfert thermique pour une configuration duale. Le sillage thermique de la source inférieure affecte de façon nette le transport depuis les sources qui sont au dessus. Le chauffoir le plus bas est marginalement influencé par la présence des chauffoirs placés au dessus.

NATÜRLICHE KONVEKTION AN ANORDNUNGEN ZWEIDIMENSIONALER WÄRMEQUELLEN IN EINEM RECHTECKIGEN HOHLRAUM

Zusammenfassung—Die natürliche Konvektion in einem abschnittsweise beheizten Hohlraum wird experimentell und theoretisch für Einzel- und Mehrfachanordnungen von Wärmequellen untersucht. Ein Mach–Zehnder-Interferometer wird dazu verwendet, das Temperaturfeld im Hohlraum sichtbar zu machen und örtliche sowie mittlere Wärmeübergangskoeffizienten an den einzelnen Wärmequellen zu bestimmen. Die partiellen Differentialgleichungen für die Erhaltung von Masse, Impuls und Energie werden für das vorliegende Problem numerisch gelöst. Die Ergebnisse zeigen, daß für einzelne Heizelemente nahe am Boden des Hohlraums die größten Wärmeübergangskoeffizienten im Bereich großer Grashof-Zahlen auftreten. Allerdings wird auch die Beobachtung in einer früheren Arbeit bestätigt, daß nämlich die Position der Wärmequelle für optimalen Wärmeübergang von der Grashof-Zahl abhängt. Auch für die Anordnung mit zwei Wärmequellen ergibt sich ein optimaler Wärmeübergang, wenn die Wärmequellen am Boden des Hohlraums positioniert werden. Das günstige Verhalten einer Anordnung der Wärmequellen (allein oder paarig) nahe dem Hohlraumboden wird durch die Intensität der Auftriebsströmung im Hohlraum erklärt. Der thermische Nachlauf einer Wärmequelle am Boden beeinflußt bei Anordnung mit mehreren Wärmequellen die Transportvorgänge im oberen Bereich beträchtlich. Die unterste Wärmequelle wird jedoch kaum durch die Anwesenheit von höher gelegenen Wärmequellen beeinflußt.

ЕСТЕСТВЕННАЯ КОНВЕКЦИЯ В ПОЛОСТИ ПРЯМОУГОЛЬНОГО СЕЧЕНИЯ, СОДЕРЖАЩЕЙ ДВУХМЕРНЫЕ ДИСКРЕТНЫЕ ИСТОЧНИКИ ТЕПЛА

Аннотация—Экспериментально и теоретически исследуется естественная конвекция в дискретно нагреваемой полости с одним или несколькими источниками тепла. Для визуализации температурного поля внутри полости и определения локальной и средней характеристик теплопереноса в случае дискретных источников тепла используется интерферометрия Маха–Цендера. Численно решаются дифференциальные уравнения в частных производных, описывающие в указанной задаче сохранение массы, импульса и энергии. Полученные результаты показывают, что приближение одиночного теплового источника ко дну полости приводит к возрастанию значения числа Грасгофа, при котором теплоперенос становится наиболее интенсивным. Тем не менее подтверждается вывод предыдущей работы о том, что соответствующее наиболее интенсивному теплопереносу расположение источника тепла зависит от числа Грасгофа. Найдено также, что расположенные вблизи дна полости дискретные источники тепла приводят к наиболее интенсивному теплопереносу в случае конфигурации нагревателя из двух источников. Оптимальное размещение нагревателей с целью создания наиболее интенсивного теплопереноса как в случае одного теплового источника, так и в случае двух тепловых источников связано с распределением интенсивности свободноконвективного потока в полости. Установлено, что тепловой след расположенного у дна полости теплового источника существенно влияет на перенос от источников тепла у крышки полости в случае нескольких тепловых источников. Однако влияние верхнего нагревателя на самый нижний источник тепла незначительно.